Topographical Effects on Turbulent Characteristics of Wind Flow over Hilly Terrain

Yutaka Hasegawa
Ecotopia Science Institute,
Nagoya University,
Furo-cho, Chikusa-ku, Nagoya 464-8603, Japan
hasegawa@mech.nagoya-u.ac.jp

Hiroshi Imamura, Koji Kikuyama, Hitoshi Suzuki, Yusuke Majima, and Yukiko Furusawa
Department of Mechanical Engineering,
Nagoya University,
Furo-cho, Chikusa-ku, Nagoya 464-8603, Japan
h044122m@mbox.nagoya-u.ac.jp

ABSTRACT

Complex terrain has become attractive as the site proposed for WTGS (Wind Turbine Generator System). The turbulent intensity of the wind flow over the complex terrain is, however, much larger than that over flat terrain, and it brings about increased aerodynamic load on the wind turbine blades. Therefore it is important for the design of WTGS and wind turbine blades to estimate and/or to measure the turbulent characteristics of the wind over complex terrain correctly.

The purpose of the present work is to clarify the topographical influence of the complex terrain on the atmospheric boundary layer flow, especially focusing on the turbulence characteristics of the wind. The detailed wind measurements using multi wind-masts were carried out at Shitara-Cho, Aichi in Japan during the period from November 19th in 2003 to March 23rd in 2004. The influence of the terrain slope on the wind has been examined by analyzing the vertical profile of mean velocity and the characteristics of the turbulence, such as the power spectrum and the coherence.

1. INTRODUCTION

In order to reduce the emission level of carbon dioxide into the atmosphere, introduction of WTGS (Wind Turbine Generator System) has been expanded over the world and complex terrain such as hilly or mountainous area has become attractive as the site proposed for WTGS. In complex terrain with rough surface, however, the intensity of wind turbulence is much larger than that in flat terrain, which makes the estimation of the wind energy resource more difficult. The intensive wind turbulence also brings about increased aerodynamic loads on the wind turbine blades and affects also the performance characteristics of the wind turbines.

There are several turbulence models such as turbulent intensity, power spectral density and coherence, whose representatives are those suggested in the IEC standard (IEC 61400-1, 1999)[1]. Most of these models, however, cannot satisfactorily describe the turbulence characteristics of the wind flow over a complex terrain, since they are basically deduced from the wind measurements over the flat terrain.

For the prediction of the aerodynamic load fluctuations on the wind turbine blade, numerical inflow models into the turbine rotors that describe the characteristics of the inflow turbulence are necessary along with the load calculation models. Veers model[2] is one of them and uses the power spectrum and coherence function of the wind turbulence as the input data. Recent investigations[3] have shown that significant discrepancy in the wind turbine fatigue loads may occur between the measurement and the simulated values, using the turbulence models suggested in the IEC standard. Therefore the assessment and the modeling of the turbulent characteristics of the wind flow have great importance for the design and installation of WTGS in the complex terrain.

The purpose of the present work is to clarify the topographical influence of the complex terrain on the atmospheric boundary layer flow, especially focusing on the turbulence characteristics of the wind flow over a hill.

The influence of the terrain slope on the turbulent characteristics has been examined by analyzing the vertical profile of mean velocity, the power spectrum and the coherence. The measurement results over the complex terrain are compared with the existing turbulence models suggested in the IEC standard.

2. DESCRIPTION OF TEST SITE

The wind measurements were carried out over a hill whose height is around 22m, located in Shitara-Cho in Japan (see Fig.1). The terrain around the test site is covered with grass surface exhibiting almost uniform roughness. The terrain has steep slope in the north and west side, and gentle one in the south and east side as shown in Fig.2. The prevailing wind direction is the north-northwest, and the mean wind speed of the site is about 5.0 m/s during winter season. The wind measurements campaign was conducted during the period from November 19th in 2003 to March 23rd in 2004.

3. MEASUREMENT METHOD

Three meteorological masts of 13.3m height were used and eleven anemometers were installed on the masts. Figure 3 shows the schematic diagram of the three meteorological masts. In order to investigate the correlation between the wind flows at the top of the hill and other positions, three masts were set in the two types of alignment. In the one alignment (denoted by Alignment A), the masts stood in a line (A-A' in Fig.1) parallel to the prevailing wind direction. In the other alignment (Alignment B), they were built in a line (B-B' in Fig.1) perpendicular to the prevailing wind direction.

In the following, the mast at the top of the hill is designated

by M. The remaining two masts in Alignment A are denoted by S1 and S2, and those in Alignment B, are named as T1and T2. Anemometers were installed at the five levels on the mast M, and three levels on the mast S1(T1) and S2(T2). At the top of each mast, 3D-type or 2D-type ultrasonic anemometers were equipped, and 3cup-type, vane-type and propeller-type anemometers were installed at the other height.

Signals from the all anemometers were sampled simultaneously, using the synchronous clock signal (see Fig.3) at 40Hz frequency. The measured wind data were divided into a set of time series of 10 minutes length, and were analyzed within each time series. The averaged wind speed, the turbulence intensity etc. were calculated over 10 minutes. For the data reduction process, bin-method was also adopted.

4. RESULTS AND DISCUSSIONS

The prevailing wind direction during the measurement campaign was found to be the north-northwest and the results of turbulence analysis shown in the following sections are based only on the wind blowing in the prevailing direction. The criteria for the data selection are as follows; the averaged wind direction over 10 minutes should be within 330°±10°. The fluctuation range of the instantaneous wind direction in 10 minutes should be within 330°±90° for Alignment A and 330°±60° for Alignment B.

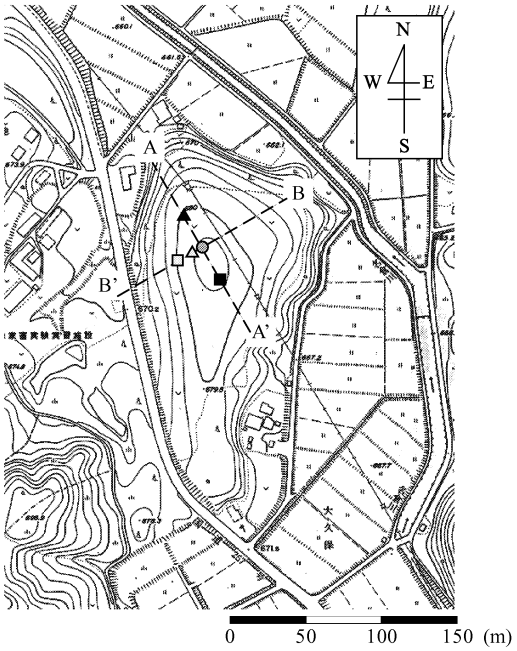

Fig.1 Topograhical map of test site

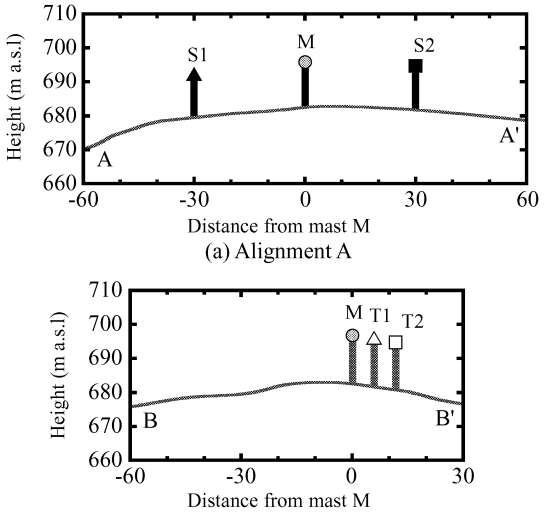

Fig.2 Terrain profile along A-A' and B-B'

4.1 VERTICAL PROFILE OF WIND SPEED

Figure 4 shows the vertical profile of the averaged wind speed at mast M, S1 and S2 in Alignment A. The wind speed is normalized by the data at the top of mast M, U_{H_M}. Lines plotted in Fig.4 are obtained by the least square approximation for the power-law defined as;

$$\frac{U(z)}{U_H} = \left(\frac{z}{H}\right)^{1/\alpha} \qquad (1)$$

where U_H is the average wind speed at the top of each mast, H is height of masts (=13.3m a.g.l.) and $1/\alpha$ is power factor.

At mast M, the averaged wind speed becomes faster than S1(the upstream mast) at all height levels due to the displacement effects of the flow by the hill, and the vertical gradient of the wind speed decreased, resulting in the increase of power factor. In the downstream at mast S2, the average wind speed decreases slightly at all height levels, which corresponds to the terrain slope.

4.2 TURBULENT INTENSITY

Figure 5 shows the distribution of turbulent intensity($=\sigma/U_H$) plotted against the horizontal mean wind speed at the top of mast M.

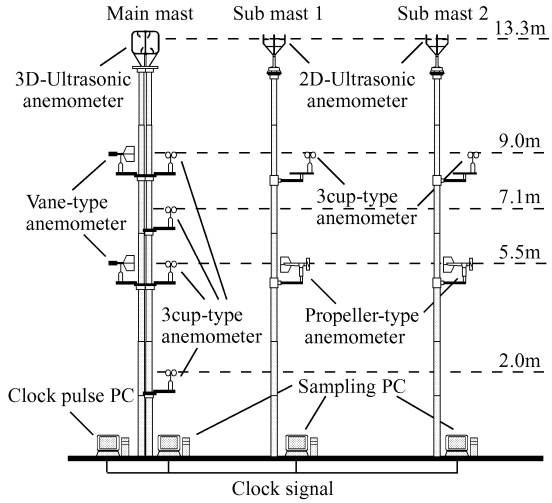

Fig.3 Schematic diagram of measurement system

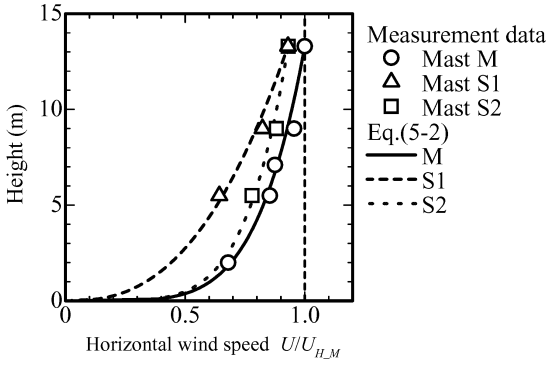

Fig.4 Vertical profile of averaged wind speed (Alignment A)

In complex terrain, turbulent intensity varies place by place, which may greatly affect the characteristics of the power output and bring about complicated aerodynamic loads on the wind turbine blades. Since the bin-averaged value does not seem to evaluate the turbulent characteristics of the site satisfactorily, the standard deviation of the turbulent intensity is added to the bin average and is plotted in Fig. 5 denoted as 'Bin-method'. For the comparison with the experimental data, IEC turbulent models, defined by the following equation (2) are also plotted by solid lines in the same figure.

$$\begin{aligned} &TI = TI_{15}\,(15/U_H + a)/(1+a) \\ &TI_{15}: TI \text{ at } U = 15\text{m/s} \\ &\text{Class A}: a = 2, TI_{15} = 18(\%) \\ &\text{Class B}: a = 3, TI_{15} = 16(\%) \end{aligned} \qquad (2)$$

where TI_{15} is the value of turbulent intensity at the wind speed of U=15m/s, U_H is 10 minutes average of wind speed at the top of mast, and a is the selected parameter for two types of class value suggested in IEC model.

When the wind speed exceeds 4m/s, the measured Bin-method value of TI becomes larger than that of Class B, and when over 6m/s, TI exceeds even that of Class A (class for large turbulent intensity). The results shown in Fig. 5 suggest that the WTGS designed on the basis on the IEC model cannot be applied to the complex terrain such as the present test site. As denoted above, the IEC turbulent model has been deduced mainly from the data for the flat terrain, and a new model suitable for the complex terrains is inevitable if the WTGS will be introduced on the hilly or mountainous site. The curve of the turbulent intensity appropriate for the present site is also drawn in Fig.5, whose parameters are compared with the values for IEC models in Table 1.

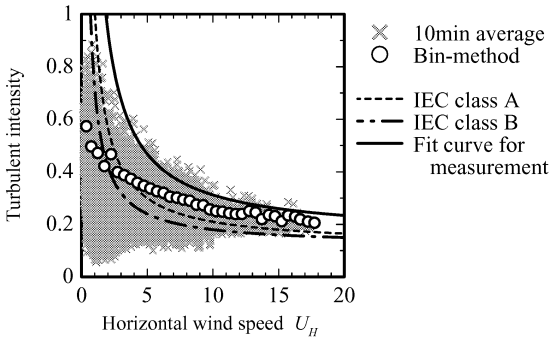

Fig.5 Distribution of turbulent intensity

Table.1 The value of parameters of the IEC model

	Class A	Class B	Fit for measurement
TI_{15}	0.18	0.16	0.26
a	2	3	1.5

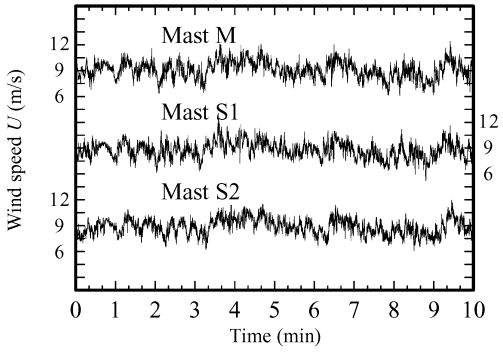

Fig.6 Time series of wind speed

4.3 CORRELATION ANALYSIS

In this section, the characteristics of the measured wind turbulence are examined by analyzing the power spectrum and the coherence for two velocity components (longitudinal component (u), lateral component (v)). By comparing the IEC models (Kaimal spectral model, Exponential coherence model) with the measurement results, validity of the models is evaluated. Since these IEC models are used for creating the inflow models in the load calculation of the wind turbine rotors, the reliability of these models has to be confirmed for the design of WTGS.

4.3.1 Characteristic Change of Prevailing Wind in Longitudinal Direction

In this section, the effects of the topography on the turbulent characteristics of prevailing wind are examined in the longitudinal direction by analyzing the power spectrum density and the coherence obtained from the measurement of Alignment A. Figure 6 shows an example of time series for the wind speed measured at three masts located in Alignment A.

Power Spectrum Density (PSD)

To examine the turbulent characteristics, the power spectrum density (PSD) was calculated by FFT method, for the fluctuation components parallel and perpendicular to the prevailing direction at the top of masts. The PSD $S_{xx}(f)$ is defined as;

$$\sigma^2 = \int_0^\infty S_{xx}(f)\,df \qquad (3)$$

where f is frequency. The calculated PSD for each time series is normalized by its standard deviation of the velocity fluctuation and frequency, and averaged by using bin-method.

Kaimal et. al.[4] proposed a PSD model defined by Eq. (4) and suggested parameters in the equation for the neutrally stable condition at flat terrain as a=105, b=33 and c=5/3.

$$\frac{fS_{xx}(f)}{\sigma^2} = \frac{an}{(1+bn)^c} \qquad (4)$$

where n is normalized frequency ($n=fH/U_H$; H : height of mast, U_H : averaged wind speed). Since there are few examples of PSD measured at the complex terrain, which are available for the comparison with the proposed PSD model, the results of PSD from our measurement are compared with Kaimal model. By using least square method, the three parameters in Eq.(4) (a, b and c) are evaluated, and the effects of terrain are examined on the characteristics of PSD.

Dimensionless frequency for the peak value in PSD, n_p, can be calculated from Eq.(4), and given as;

$$n_p = \frac{f_p H}{U_H} = \frac{1}{b(c-1)} \qquad (5)$$

Figure 7 shows the dimensionless PSD obtained from the measurement of Alignment A [Figure 7(a) for the longitudinal fluctuation component (u) and Fig. 7(b) for the lateral component (v)] when the average wind speed at the top of mast M is within 9±0.5m/s. The PSD approximated by Eq. (4), the peak dimensionless frequency, n_p, and the power factor, c, are also plotted in the same figure.

In case of the along-wind component (u), the values of n_p and c are the lowest at mast M (at the top of the hill), and are higher at S1 (upstream of the hill-top) than those at S2 (downstream of the hill-top). In case of the across-wind component (v), however, n_p at mast S1 shows slightly lower frequency than that of S2. From these results, it can be said that the PSD of the turbulent velocity fluctuation is closely related to the topographical gradient of the terrain, although effects of the terrain slightly

differ with the direction of the fluctuation component.

Using the dimensionless frequency for the peak value in PSD, n_p, a representative scale of the turbulent fluctuation, L_p, can be deduced for the flow around the hill as;

$$L_p \cong \frac{U_H}{f_p} = \frac{U_H}{n_p U_H / H} = \frac{H}{n_p} \tag{6}$$

Figure 8 shows the turbulence scale L_p for the along-wind component plotted against the averaged wind speed. As the prevailing wind climbs the steep slope to the top of the hill (mast M) from the upstream (mast S1), the turbulence scale is increased significantly, which suggests the occurrence of the vortex stretching around the top of the hill. In the downstream from mast M to mast S2, where gentle slope exits, the scale L_p is almost unchanged and takes the value similar to Kaimal model as shown in Fig. 8.

The slight dependence of the scale on the wind speed can be found especially at mast S1 (on the steep slope), that is, the scale seems to shrink with the increase of wind speed. These kinds of scale dependency on the wind speed have not been considered in IEC models, and should be taken into account carefully for the complex terrain.

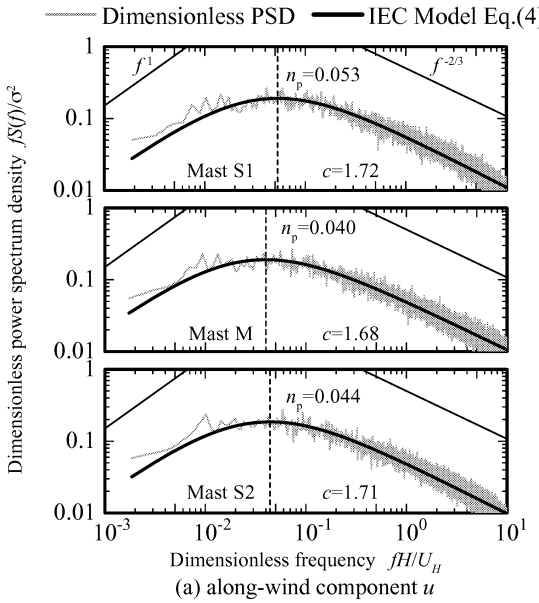

(a) along-wind component u

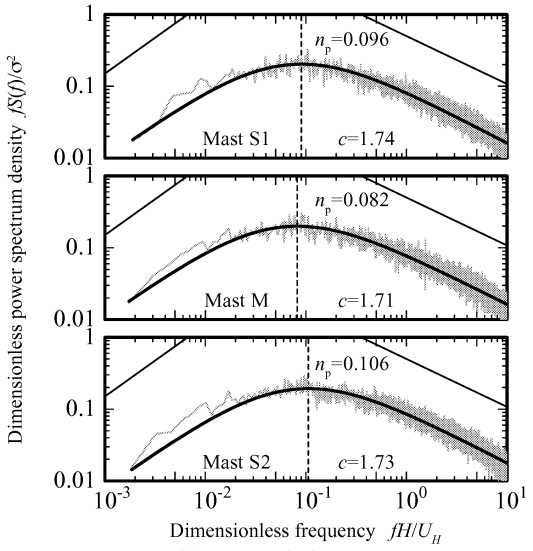

(b) across-wind component v

Fig.7 Power spectrum density

It should be also noted that obtained value of L_p is above 100m at any position, which fully covers the distance between masts in Alignment A, equipped within 60m.

Coherence

The coherence of the wind fluctuations between the different positions is calculated by means of the following equation.

$$\gamma^2(f) = \frac{|S_{xy}(f)|^2}{S_{xx}(f) S_{yy}(f)} \tag{7}$$

where S_{xx}, and S_{yy} are the spectra at two points, and S_{xy} is the cross-spectrum between the two points.

Figure 9 shows the squared coherence γ^2 obtained from the measurement of alignment A [Figure 9(a) for the along-wind component (u) and Fig. 9(b) for the across-wind component (v)], in the condition that the average wind speed is within 9±0.5m/s and the wind is blowing in the prevailing direction (around 330deg). The frequency is normalized by the averaged wind speed, U_{H_M}, at the top of mast M and the distance r between the selected two masts. Three pairs of the masts are adopted for the calculation, that is, M-S1, M-S2 and S1-S2. The distances for the pairs are r=30m or 60m.

From Fig. 9, the coherency for M-S1 and M-S2 are nearly

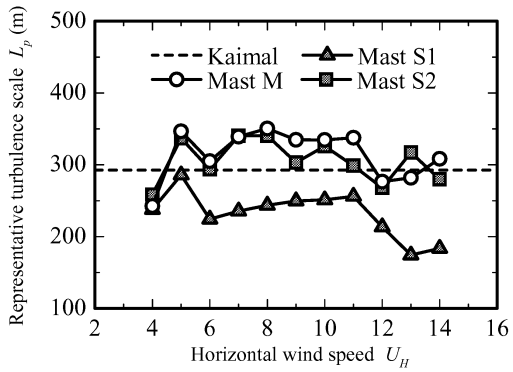

Fig.8 Distribution of representative turbulence scale of along-wind component

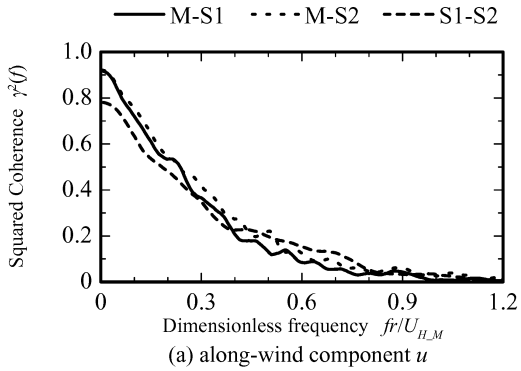

(a) along-wind component u

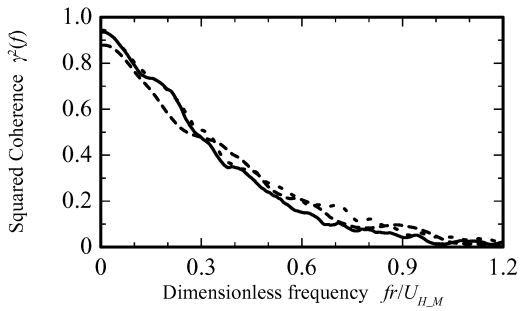

(b) across-wind component v

Fig.9 Measured coherence for longitudinal separation

equal and higher than that for S1-S2, in the low frequency region, which can be attributed directly to the distance between the masts. That is, the coherence for the longer distance shows the lower level. It is also indicated from the comparison between M-S1 and M-S2, that there is no large effect on the coherence from the variation of the topographical gradient. The representative scale of the turbulence is larger than the total distance between masts, as shown in Fig. 8, which might be the reason why the effect of topographical gradient does not appear in the coherence.

Concerning about the effects due to different velocity components, the coherence of *u*-component decays faster than that of *v*-component, not only with the increase of the frequency but with the increase of separation, showing the directional dependency of the turbulent characteristics.

4.3.2 Characteristic Change of Prevailing Wind in Lateral Direction

In this section, variation of the turbulence characteristics is analyzed in the direction lateral to the prevailing wind, by examining the measurement results obtained from the masts installed in Alignment B. The power spectrum density and the coherence obtained from the measurements are compared with the IEC models, and validity of the IEC models will be discussed. Figure 10 shows an example of time series for the wind speed measured at Alignment B.

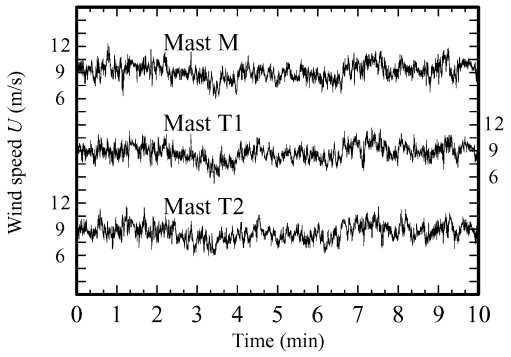

Fig.10 Time series of wind speed

Power Spectrum Density (PSD)

Figure 11 shows the dimensionless PSD for *u*-component obtained from the measurement of alignment B, when the wind is blowing in the prevailing direction and the average speed is within 9±0.5m/s at the top of mast M. The figure also includes the PSD model approximated by Eq.(4), the peak dimensionless frequency n_p and power factor *c*.

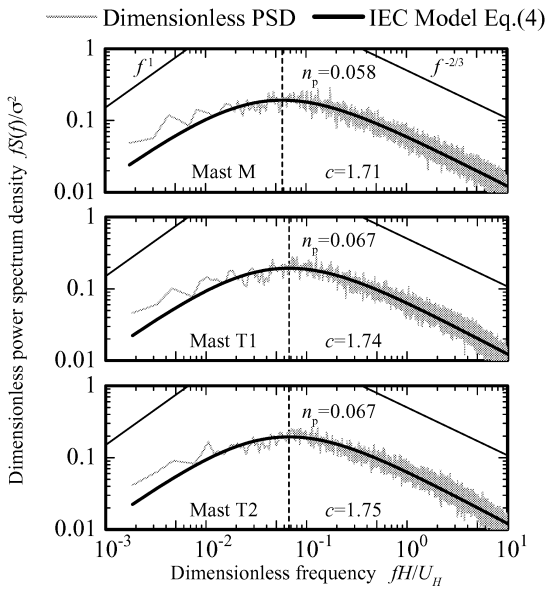

Fig.11 Power spectrum density of along-wind component *u*

The peak frequency n_p at mast M shows smaller value than those at T1 and T2, and the factor *c* takes its minimum at mast M. Figure 12 shows the turbulence scale L_p defined by Eq.(6), for the along-wind component plotted against the averaged wind speed. The turbulence scale at mast M is the largest among the masts for Alignment B. By considering these results along with the topographical gradient around the masts, it can be said that the steepness of the slope in the streamwise direction affects the shape of power spectrum density and changes the scale of the turbulence.

In contrast to the results for Alignment A, the representative scale seems hardly to vary with the wind speed. It should be also noted that the scale at mast M for Alignment B is slightly smaller than the value of Kaimal model and the results for Alignment A. The measurement for Alignment A and B were carried out in the different periods (Alignment A: from November 9th to December 10th in 2003, Alignment B: from December 11th in 2003 to March 23rd in 2004), so that the difference in the atmospheric stability condition probably brought about effects on the structure of the turbulence.

Coherence

The squared coherence γ^2 for the along-wind component obtained from Alignment B is plotted in Fig. 13, in the condition that the averaged wind speed is within 9±0.5m/s and the wind is blowing in the prevailing direction (around 330deg). The results for three pairs of the masts are included in the figure, that is, M-T1, M-T2 and T1-T2, where the distances between the masts are *r*=6m or 12m.

The tendency of the coherence in the lateral direction is found to be quite different from the longitudinal coherence, if Fig. 13 is compared with Fig.9(a). Considering the distances between

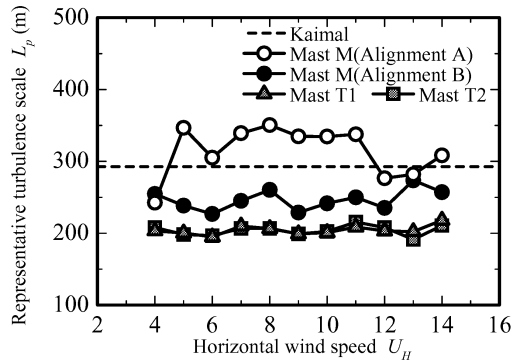

Fig.12 Distribution of representative turbulence scale for Alignment B

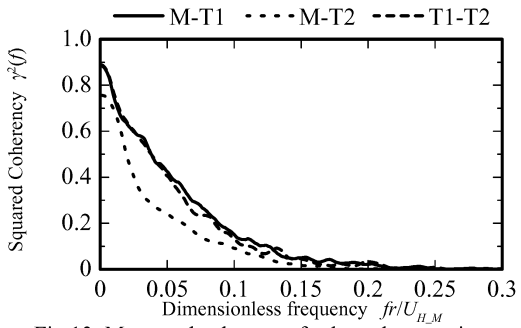

Fig.13 Measured coherence for lateral separation

the masts for Alignment A an B, the effect of lateral separation is much larger than the longitudinal separation. Additionally, the coherence value decays with the frequency significantly faster for the case of lateral separation.

For the coherence of lateral separation, the exponential coherence model is suggested by the IEC standard as;

$$\gamma^2(f) = \left[\exp\left\{-8.8\sqrt{(fr/U_H)^2 + (0.12r/L_c)^2}\right\}\right]^2 \qquad (8)$$

where f is frequency, r is distance and L_c is scale parameter. Using the suggested value for scale, as $L_c = 32.6$, the above equation is plotted in Fig. 14 and compared with the measurement results for the mast pair of M-T2. Although the IEC coherence model has been widely used to produce numerical inflow models into the turbine rotors, it cannot sufficiently describe the coherence of the wind turbulence in complex terrain, as shown in Fig. 14. So that modification of the IEC model is attempted[5] by adding an decay parameter a along with the scale parameter L as follows.

$$\gamma^2(f) = \left[\exp\left\{-a\sqrt{(fr/U_H)^2 + (0.12r/L)^2}\right\}\right]^2 \qquad (9)$$

Two parameters a and L in Eq. (9) are calculated by least-square method based on the wind measurement. The approximated curve by Eq. (9) is compared with the measured data and IEC model Eq. (8) in Fig.14. Equation (9) fits the measurement much better than Eq. (8) in its absolute value and characteristics of frequency decay.

Figure 15(a) and (b) show the calculated values of decay parameter a and scale parameter L, respectively, plotted against the averaged wind speed. The decay parameter seems to have little dependency on the wind speed, while it increases with the lateral separation. The scale parameter varies significantly both with the changes in the wind speed and the selected pairs of masts. These results suggest that the modified model by Eq. (9) is convenient to evaluate the characteristics of the coherence at complex terrain by examining the parameters, although further modification of the model is necessary if it will be used for the production of the numerical inflow model into the turbine rotor.

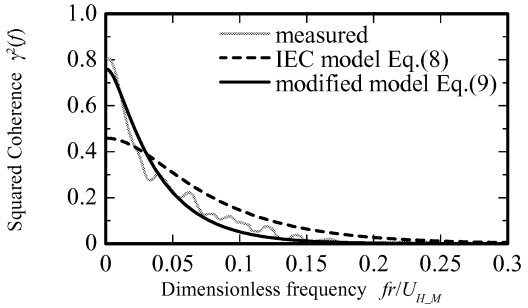

Fig.14 Comparison of UEC and modified IEC models with measured lateral coherence of u-component

5. CONCLUSIONS

The detailed wind measurements have been conducted at Shitara-cho, Aichi in Japan, and results of measurements have been compared with current turbulent models. The major results obtained in this study are as follows;

- The effect of the displacement by a hill on the wind speed is confirmed by examining the vertical profile of the wind speed.
- When the slope of the complex terrain is steep, turbulent intensity becomes larger than the current IEC turbulent models, and the peak frequency of the power spectrum density, and thus the representative turbulence scale, differ from those for the flat terrain, depending upon the topographical conditions.
- The topographical effects on the spatial correlation of the wind velocity have been examined by using the coherence function. The coherence for the longitudinal separation is found to be larger than that for the lateral separation. Since the representative scale of the turbulence overcomes the total distance between the meteorological masts, the effect of topographical gradient does not clearly appear in the results of the coherence.
- The IEC exponential coherence model is not valid for the present site, and modification of the model has been attempted, by adding an extra parameter.

REFERENCES

[1] IEC 61400-1, Wind turbine generator systems- Part1 : Safety requirements, second edition, 1999-02

[2] Veers, P. S., "Three-Dimensional Wind Simulation", SAND-88-0152, Sandia National Laboratories, (1988).

[3] Imamura, et. al. "Study on the Wind Measurements and Performance Evaluation of a WTGS in Complex Terrain (2nd report, Effect of Wind Characteristics and Turbulent Intensity)", in Japanese, JSME Vol70-693-B, pp1223-1229 (2004)

[4] Kaimal, J.C, et. al. "Spectral characteristics of surface layer turbulence", Q.J.R. Meteorology, 98, (1972), pp563-589

[5] Korn Saranyasoontorn, Lance Manuel, Paul S. Veers, "A Comparison of standard coherence models for inflow turbulence with estimates from field measurements", University of Texas at Austin, Austin, Sandia National Laboratories, Albuquerque, (2004)

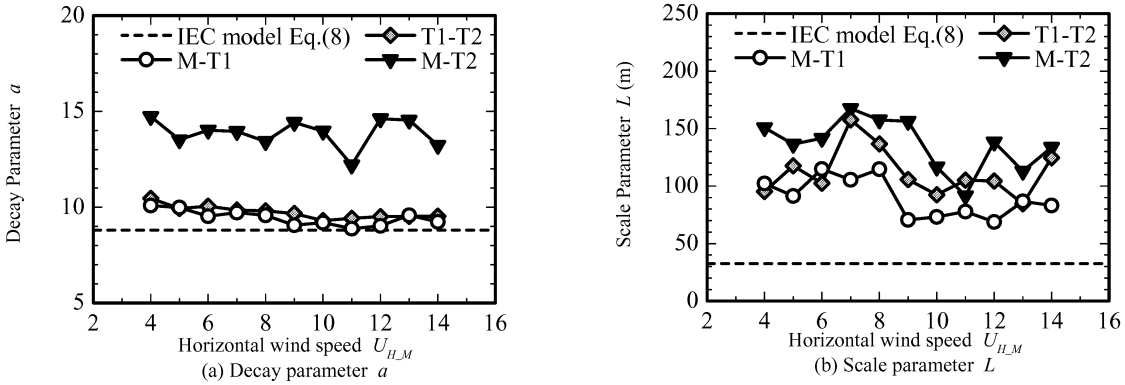

Fig.15 Variation of decay parameter a and scale parameter L in modified IEC model